Journal of Applied Electrochemistry (2005) 35:1171–1181
DOI 10.1007/s10800-005-9030-x

Macrokinetic analysis of polarisation characteristics of gas-diffusion electrodes in contact with liquid electrolytes, Part II: Oxygen reduction as example for a higher order reaction

KAI SUNDMACHER[1,2,*] and THORSTEN SCHULTZ[1]
[1]*Max-Planck-Institut für Dynamik komplexer technischer Systeme, Sandtorstraße 1, 39106, Magdeburg, Germany*
[2]*Lehrstuhl für Systemverfahrenstechnik, Otto-von-Guericke Universität Magdeburg, Universitätsplatz 1, 39106, Magdeburg, Germany*
*(*author for correspondence, tel.: +49-391-6110-351, fax: +49-391-6110-353, e-mail: sundmacher@mpi-magdeburg.mpg.de)*

Received 5 November 2004; accepted in revised form 18 May 2005

Key words: electrochemical absorption, electrochemical oxidation, gas diffusion electrode, hydrogen peroxide, modeling, oxygen cathode, partial oxidation

Abstract

Classical partial oxidation processes often suffer from low selectivities. Promising alternatives are electrochemical processes where the oxidation takes place at a packed-bed anode while an oxygen-consuming gas–liquid membrane is used as cathode. As a basis for the reliable design of such a process, the performance of oxygen-consuming gas-diffusion electrodes (GDE) is investigated experimentally and is analysed based on a rigorous model accounting for the reaction microkinetics and all relevant mass and charge transport phenomena. The results indicate that oxygen is transported in the gas-filled pores by Knudsen diffusion and that the cathodic oxygen reduction follows a parallel reaction scheme forming hydrogen peroxide at the carbon black support and water at the applied platinum catalyst particles.

List of symbols

ai_0	A m^{-3}	exchange current density with respect to electrode volume
B_1, B_2	1	dimensionless parameter groups
Bi_m	1	Biot mass number (Table 1)
c	mol m^{-3}	concentration in liquid phase
d	m	thickness of electrode
d^*	1	dimensionless thickness of flooded layer (Table 1)
D^*	1	ratio of mass transport resistances (Table 1)
D	m^2 s^{-1}	diffusion coefficient
e	1	effective ratio of reactants with respect to bulk phase conditions (Table 1)
E	1	enhancement factor of electrochemical reaction (Table 1)
F	C mol^{-1}	Faraday constant, $=96485$ C mol^{-1}
H	Pa	Henry coefficient
Ha	1	Hatta number (Table 1)
i	A m^{-2}	current density
k	m s^{-1}	mass transfer coefficient
n	1	number of transferred electrons
p	Pa	pressure in gas phase
r	m	length coordinate through pore (Figure 2)
R	J mol^{-1} K^{-1}	universal gas constant, $=8.314$ J mol^{-1} K^{-1}
s	1	stoichiometric coefficient in ionic molecule
T	K	temperature
u	mol m^2 J^{-1} s^{-1}	ionic mobility
U	V	electrode potential vs. standard hydrogen electrode
z	1	charge number
α	1	charge transfer coefficient
β	1	Prater number of electrochemical reaction (Table 1)
ε	1	porosity (void fraction) of electrode
κ	$(\Omega$ m$)^{-1}$	ionic conductivity of electrolyte
ϕ	V	electric potential
ν	1	stoichiometric coefficient in reaction
η	V	overpotential

ρ	1	electrolyte resistance
σ	$(\Omega\ m)^{-1}$	ionic conductivity of solid phase

Upper indices

dir	direct reaction path of oxygen reduction
e	in equilibrium
FL	in flooded layer of the electrode (Figure 2)
G	in gas film (Figure 2)
GL	in gas-filled layer of the electrode (Figure 2)
ind	indirect reaction path of oxygen reduction
L	in liquid film (Figure 2)
S	in solid phase
*	dimensionless

Lower indices

a	anodic
c	cathodic
counterion	counterion in electrolyte
eff	effective
H^+	protons
i	of the instantaneous reaction
j	component index
$i = 0$	at zero current (open circuit)
lim	limiting
max	maximum
n	normal to solid surface, towards electrolyte
O_2	oxygen
RE	reference electrode
t	total

1. Introduction

In the early 1980s it was suggested that oxygen-consuming electrodes might be used as counter electrodes in chlorine production, instead of hydrogen-producing electrodes [1, 2]. This would lead to lower energy and safer operation, as hydrogen is highly explosive, especially when accidentally mixed with chlorine. Other possible applications are as counter electrodes in the production of metal solutions (e.g. $Sn(BF_4)_2$) for electro-plating [3] and in electrochemical hydrocarbon partial oxidation processes in the liquid phase [4–7].

Finally, and maybe most importantly, oxygen cathodes play a major role in all types of fuel cells. Also here the mechanisms of oxygen conversion (i.e. the electrocatalysis) and the role of mass transport of oxygen and the reaction products (e.g. water) needs to be fully understood. Such knowledge is essential for further optimisation of fuel cell performance. In this field a large number of recent publications are available. For a good overview see e.g. [8].

As a basis for the reliable design of such processes, the performance of the oxygen-reducing GDE is investigated experimentally and analysed on the basis of a rigorous model which accounts for the reaction microkinetics as well as for all relevant mass and charge transport phenomena.

Figure 1 shows a schematic of such a GDE: Oxygen is transported to the electrode surface through the outer gas film (step 1), diffuses through a pore (step 2) to the gas–liquid interface and is then absorbed in the liquid phase (step 3). The absorbed oxygen diffuses through the liquid phase (step 4) to the reaction zone (step 5). Simultaneously protons are transported from the liquid bulk through the outer liquid film (step 7) and the flooded part of the pore (step 6). In the reaction zone (step 5), oxygen, protons and electrons (step 8) react to form water. As water is the main component of the liquid phase, its transport out of the pore has little impact on the other transport processes. Therefore, it is neglected in the further analysis.

The GDEs used for the experiments consisted of platinum catalyst supported on carbon black (total platinum loading 1.5 mg cm^{-2}), carbon black without catalyst loading and a polymeric binder (PTFE). A detailed description of the production process as well as information on the physical properties of the GDEs can be found in [9, 10].

2. Process analysis

In the following, a mathematical model for the simulation of polarisation curves of GDEs will be derived, based on an approach previously developed for first-order reactions [11]. In order to obtain a compact model formulation, dimensionless variables and parameter groups are introduced, marked with the upper index "*". They are listed and explained in Table 1.

The electrochemical oxygen absorption reaches a maximum value of the current density, $i_{\mathrm{eff,\ max}}$ [A m^{-2}], when only the oxygen diffusion in the gas filled part of the pores (the gas layer, step 2 in Figure 1) is the rate limiting step:

$$i_{\mathrm{eff,max}} = nF\frac{N^{\mathrm{GL}}_{\mathrm{O_2,max}}}{\nu_{\mathrm{O_2}}} = -nF\frac{D^{\mathrm{GL}}_{\mathrm{eff,O_2}}}{d^{\mathrm{GL}}}\frac{p^{\mathrm{G}}_{\mathrm{O_2}}}{RT} \tag{1}$$

Here n [–] is the number of transferred electrons per net reaction, $F = 96485$ C mol^{-1} is Faraday's constant, $N^{\mathrm{GL}}_{\mathrm{O_2,max}}$ [mol m^{-2} s^{-1}] is the maximum oxygen molar flux density, $D^{\mathrm{GL}}_{\mathrm{eff,O_2}}$ [m^2 s^{-1}] is the effective oxygen diffusion coefficient in the gas layer (GL), d^{GL} [m] is its thickness, $p^{\mathrm{G}}_{\mathrm{O_2}}$ [Pa] is the oxygen partial pressure in the gas film (G), $R = 8.314$ J mol^{-1} K^{-1} is the universal gas constant and T[K] is the gas temperature.

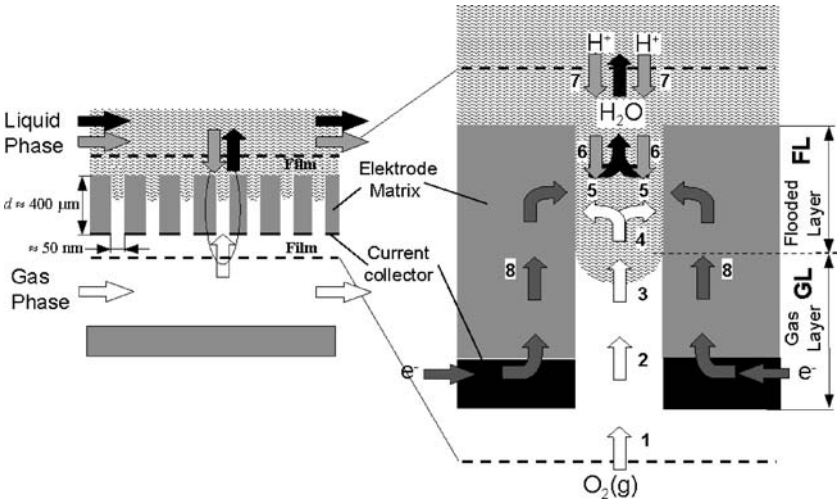

Fig. 1. Structure of gas diffusion electrode (GDE) and transport phenomena occurring for oxygen absorption.

Table 1. Definition and interpretation of dimensionless parameter groups

	Definition	Physical meaning
Biot mass number for gas phase	$\mathrm{Bi}_\mathrm{m}^\mathrm{G} \equiv \frac{k_{\mathrm{O}_2}^\mathrm{G} d}{D_{\mathrm{eff},\mathrm{O}_2}^\mathrm{GL}}$	$= \frac{\text{mass transfer in G}}{\text{pore diffusion velocity in GL}}$
Biot mass number for liquid phase	$\mathrm{Bi}_\mathrm{m}^\mathrm{L} \equiv \frac{k_{\mathrm{O}_2}^\mathrm{L} d}{D_{\mathrm{eff},\mathrm{O}_2}^\mathrm{FL}}$	$= \frac{\text{mass transfer in L}}{\text{pore diffusion velocity in FL}}$
Thickness of flooded layer (FL) of electrode	$d^* \equiv \frac{d^\mathrm{FL}}{d}$	$= \frac{\text{thickness of FL}}{\text{total electrode thickness}}$
Ratio of mass transport resistances (GL/FL)	$D^* \equiv \frac{D_{\mathrm{eff},\mathrm{O}_2}^\mathrm{FL} c_{\mathrm{O}_2}^\mathrm{Le}(p_{\mathrm{O}_2}^\mathrm{G})}{D_{\mathrm{eff},\mathrm{O}_2}^\mathrm{GL}(p_{\mathrm{O}_2}^\mathrm{G}/RT)}$	$= \frac{\text{pore diffusion velocity in FL}}{\text{pore diffusion velocity in GL}}$
Effective reactant ratio with respect to bulk phases	$e \equiv \frac{c_{\mathrm{O}_2}^\mathrm{Le}(p_{\mathrm{O}_2}^\mathrm{G})/\nu_{\mathrm{O}_2}}{c_{\mathrm{H}^+}^\mathrm{L}/\nu_{\mathrm{H}^+}}$	$= \frac{\mathrm{O}_2 \text{ concentration at } p_{\mathrm{O}_2}^\mathrm{G} \text{ in liquid phase}}{\mathrm{H}^+\text{concentration in L}}$
Enhancement factor of electrochemical reaction	$E \equiv \frac{\tilde{H}a}{\tanh \tilde{H}\alpha} \approx \tilde{H}a; \tilde{H}a \equiv d^* Ha \exp(-0.5\alpha_c \eta^*)$	$= \frac{\mathrm{O}_2 \text{ absorption with reaction}}{\mathrm{O}_2 \text{ absorption without reaction}}$
Enhancement factor of instantaneous reaction	$E_i \equiv 1 + \frac{\nu_{\mathrm{O}_2} D_{\mathrm{eff},\mathrm{H}^+}^\mathrm{FL} c_{\mathrm{H}^+}^i}{\nu_{\mathrm{H}^+} D_{\mathrm{eff},\mathrm{O}_2}^\mathrm{FL} c_{\mathrm{O}_2}^\mathrm{Le}(p_{\mathrm{O}_2}^\mathrm{G})}$	$= \frac{\mathrm{H}^+ \text{ pore diffusion velocity in FL}}{\mathrm{O}_2 \text{ pore diffusion velocity in FL}}$
Hatta number	$Ha \equiv d\sqrt{\frac{a i_0/(nF)}{D_{\mathrm{eff},\mathrm{O}_2}^\mathrm{FL} c_{\mathrm{O}_2}^\mathrm{Le}(p_{\mathrm{O}_2}^\mathrm{G})}}$	$= \frac{\text{reaction rate with respect to L}}{\text{pore diffusion velocity in FL}}$
Effective current density	$i_\mathrm{eff}^* \equiv \frac{i_\mathrm{eff}}{i_\mathrm{eff,max}}$	$= \frac{\text{effective current density}}{\text{maximum effective current density}}$
Prater number of electrochemical reaction	$\beta \equiv \frac{nF^2 D_{\mathrm{eff},\mathrm{O}_2}^\mathrm{FL} c_{\mathrm{O}_2}^\mathrm{Le}(p_{\mathrm{O}_2}^\mathrm{G})}{\sigma_\mathrm{eff}^\mathrm{S} RT}$	$= \frac{\text{pore diffusion velocity in FL}}{\text{electron transport in S}}$
Electric resistance of electrolyte	$\rho^* \equiv \frac{D_{\mathrm{eff},\mathrm{O}_2}^\mathrm{GL} p_{\mathrm{O}_2}^\mathrm{G} d^\mathrm{RE} nF^2}{\kappa^\mathrm{L} d^\mathrm{GL} (RT)^2}$	$= \frac{\text{pore diffusion velocity inGL}}{\text{charge transport in L}}$
Total overpotential	$\eta^* \equiv \frac{F}{RT}(U - U_{i=0}^i)$	

This maximum effective current density is used to formulate the dimensionless current densities according to Table 1.

2.1. *Model for electrochemical gas absorption in gas diffusion electrodes*

2.1.1. *Mass transport*

Figure 2 shows schematically the qualitative reactant profiles within a pore of the electrode for low current densities (i.e. slow reaction). As the main transport resistances are expected within the flooded layer of the pore, the concentration profiles within the outer gas and liquid film, respectively, as well as within the gas layer within the electrode are assumed to be linear. The following expressions describe the molar flux densities N_j [mol m^{-2} s^{-1}] in these layers, assuming Fickian diffusion:

$$\text{Liquid film (L):} \quad N_j^\mathrm{LS} = k_j^\mathrm{L}(c_j^\mathrm{L} - c_j^\mathrm{LS}); \quad j = \mathrm{O}_2, \mathrm{H}^+ \tag{2}$$

$$\text{Gas film (G):} \quad N_j^\mathrm{GS} = k_j^\mathrm{G}\frac{p_j^\mathrm{G} - p_j^\mathrm{GS}}{RT}; \quad j = \mathrm{O}_2 \tag{3}$$

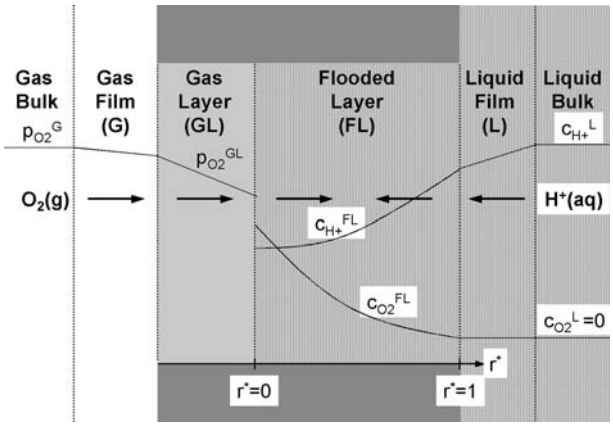

Fig. 2. Qualitative oxygen and proton concentration profiles in GDE.

$$\text{Gas layer (GL):}\quad N_j^{\mathrm{GL}} = \frac{D_{\mathrm{eff},j}^{\mathrm{GL}}}{d^{\mathrm{GL}}}\frac{(p_j^{\mathrm{GS}} - p_j^{I})}{RT};\quad j = \mathrm{O_2} \tag{4}$$

In these equations, c_j [mol m^{-3}] are molar concentrations in the liquid phase, p_j [Pa] are partial pressures in the gas phase, and k_j [m s^{-1}] are mass transfer coefficients.

Within the gas layer, mass transport is not only driven by molecular diffusion, but also by Knudsen diffusion. The superposition of both mechanisms can be described by an effective diffusion coefficient $D_{\mathrm{eff},j}^{\mathrm{GL}}$

$$\frac{1}{D_{\mathrm{eff},j}^{\mathrm{GL}}} = \frac{1 - p_j^{\mathrm{G}}/p^{\mathrm{G}}}{D_{\mathrm{eff},j}^{\mathrm{G}}} + \frac{1}{D_{\mathrm{eff},j}^{K}} \tag{5}$$

calculated from the effective diffusion coefficients in the (free) gas phase, $D_{\mathrm{eff},j}^{\mathrm{G}}$, and the effective Knudsen diffusion coefficient $D_{\mathrm{eff},j}^{K}$.

The gaseous reactant (oxygen) dissolves in the liquid phase at the gas–liquid interface. This process is assumed to be in equilibrium, and the concentration on the liquid phase side, c_j^{Le}, is calculated from the partial pressure on the gas phase side, p_j^{G}, according to Henry's law:

$$p_j^{\mathrm{G}} = H_j\, c_j^{\mathrm{Le}}/c_{\mathrm{t}}^{\mathrm{L}} \tag{6}$$

where H_j [Pa] is the Henry coefficient and $c_{\mathrm{t}}^{\mathrm{L}}$ is the total concentration in the liquid phase.

Within the flooded layer, mass transport can take place due to diffusion and electro-migration. The latter is driven by the gradient of the electric potential, ϕ^{FL} [V], and only affects charged species:

$$N_j^{\mathrm{FL}} = -D_{\mathrm{eff},j}^{\mathrm{FL}}\frac{\mathrm{d}c_j^{\mathrm{FL}}}{\mathrm{d}r} - z_j u_{\mathrm{eff},j}^{\mathrm{FL}} F c_j^{\mathrm{FL}}\frac{\mathrm{d}\phi^{\mathrm{FL}}}{\mathrm{d}r};\quad j = \mathrm{O_2}, \mathrm{H^+} \tag{7}$$

Here z_j [–] is the charge number of species j, $u_{\mathrm{eff},j}^{\mathrm{FL}}$ [mol m^2 J^{-1} s^{-1}] is its ionic mobility and r [m] is the spatial coordinate (see Figure 2).

Equation (7) is only valid for dilute electrolytes. To account for the porosity ε [–] of the electrode, the following approximation for the molecular transport coefficients were used (as proposed e.g. by Newman [12]):

$$D_{\mathrm{eff},j}^{\mathrm{G}} = \varepsilon^{1.5} D_j^{\mathrm{G}},\quad D_{\mathrm{eff},j}^{\mathrm{FL}} = \varepsilon^{1.5} D_j^{\mathrm{L}},\quad u_{\mathrm{eff},j}^{\mathrm{FL}} = \varepsilon^{1.5} u_j^{\mathrm{L}} \tag{8}$$

For the model, water is not accounted for as it is the excess component in the liquid phase and should therefore have no significant influence on the overall process.

Finally, in the flooded layer mass balances for oxygen and protons, as well as the charge balance, are formulated in terms of the dimensionless numbers given in Table 1:

$$\text{Oxygen:}\quad \frac{\mathrm{d}^2 c_{\mathrm{O_2}}^*}{\mathrm{d}r^{*2}} = -(\mathrm{d}^* Ha)^2 i_n^* \tag{9}$$

$$\text{Protons:}\quad \frac{\mathrm{d}^2 c_{\mathrm{H^+}}^*}{\mathrm{d}r^{*2}} = -4\frac{(\mathrm{d}^* Ha)^2}{E_i - 1} i_n^* \tag{10}$$

The factor 4 in Equation (10) results from the stoichiometry of the electrochemical oxygen reduction:

$$\mathrm{O_2(g)} + 4\mathrm{e^-} + 4\mathrm{H^+} \rightarrow 2\mathrm{H_2O} \tag{11}$$

E_i [–] stands for the enhancement factor of the instantaneous reaction (i.e. maximum current density, reaction takes place in a planar reaction zone within the flooded layer).

The dimensionless boundary conditions for the oxygen balance are:

$$-\left.\frac{\mathrm{d}c_{\mathrm{O_2}}^*}{\mathrm{d}r^*}\right|_{r^*=0} = \frac{1 - c_{\mathrm{O_2}}^*(r^* = 0)}{\frac{D^*}{\mathrm{Bi}_{\mathrm{m}}^{\mathrm{G}} d^*} + \frac{D^*(1-d^*)}{d^*}} \tag{12}$$

$$-\left.\frac{\mathrm{d}c_{\mathrm{O_2}}^*}{\mathrm{d}r^*}\right|_{r^*=1} = \frac{c_{\mathrm{O_2}}^*(r^* = 1) - c_{\mathrm{O_2}}^{*\mathrm{L}}}{\frac{1}{\mathrm{Bi}_{\mathrm{m}}^{\mathrm{L}} d^*}} \tag{13}$$

Pore diffusion in the gas layer is described by D^*, the mass transport resistances in the outer liquid and gas film are accounted for by the respective Biot numbers, $\mathrm{Bi}_{\mathrm{m}}^{\mathrm{G}}$ and $\mathrm{Bi}_{\mathrm{m}}^{\mathrm{L}}$. In the same manner, boundary conditions can be formulated for the proton mass balance:

$$-\left.\frac{\mathrm{d}c_{\mathrm{H^+}}^*}{\mathrm{d}r^*}\right|_{r^*=0} = 0 \tag{14}$$

$$-\left.\frac{\mathrm{d}c_{\mathrm{H^+}}^*}{\mathrm{d}r^*}\right|_{r^*=1} = \frac{\mathrm{Bi}_{\mathrm{m}}^{\mathrm{L}} d^*}{e(E_i - 1)}(c_{\mathrm{H^+}}^*(r^* = 1) - 1) \tag{15}$$

with e being the effective ratio of both reactants related to the bulk phase conditions, taking into account the respective concentrations and stoichiometric coefficients:

$$e \equiv \frac{c_{O_2}^{Le}(p_{O_2}^{G})/(-1)}{c_{H+}^{L}/(-4)}. \tag{16}$$

2.1.2. *Charge transport*

Charge transport takes place in the solid matrix of the GDE (electron transport) as well as in the electrolyte (ion transport). Within the solid matrix, charge transport is assumed to follow Ohm's law

$$i^{S} = -\sigma_{eff}^{S}\frac{d\phi^{S}}{dr}. \tag{17}$$

The effective conductivity of the porous matrix is approximated by

$$\sigma_{eff}^{S} = (1-\varepsilon)^{1.5}\sigma^{S}. \tag{18}$$

Charge transport within the electrolyte can be described by Faraday's law accounting for the fluxes of all charged species:

$$i^{FL} = F\sum_{j=1}^{N} z_j N_j^{FL}; \quad j = H^+, \text{ counterion} \tag{19}$$

The charge balance for the solid matrix can be formulated as

$$\frac{di^{S}}{dr} = -ai_n \tag{20}$$

where a [$m^2\ m^{-3}$] is the volume-related inner electrode surface, and i_n [$A\ m^{-2}$] is the local current density normal to the inner solid surface.

For the electrolyte in the flooded electrode layer, electroneutrality is assumed:

$$\sum_{j=1}^{N} z_j c_j^{FL} = 0. \tag{21}$$

This assumption is only strictly valid for the core of the electrolyte phase, not for the electrochemical double layer. But it is justified, as long as the total volume of the double layer is small compared to the total volume of the pore liquid. However, for highly porous systems, significant deviations from electroneutrality can occur. The same is true for highly dilute electrolytes, where the double layer thickness can reach values of more than 10 nm.

For a binary electrolyte, accounting for the stoichiometric factors s_{H^+} and $s_{counterion}$ of the two ionic species within the electrolyte molecules, the molar electrolyte concentration is given by

$$c^{FL} = \frac{c_{H^+}^{FL}}{s_{H^+}} = \frac{c_{counterion}^{FL}}{s_{counterion}}. \tag{22}$$

This equation couples the concentration profiles of the two ionic species in the electrolyte and therefore the concentration of the non-reactive of the two species (counterion) can be eliminated. Its molar flux density is constant throughout the pore and equal to the value at the gas–liquid interface. For the molar flux densities of the two ionic species, one consequently gets the following expression:

$$N_j^{FL} = -D_{eff,2}^{FL}s_j\frac{dc^{FL}}{dr} - z_j u_{eff,j}^{FL}Fs_j c^{FL}\frac{d\phi^{FL}}{dr}; \quad j = H^+, \text{ counterion} \tag{23}$$

From this, the profile of the electrical potential (concentration overpotential) can be derived as a function of the concentration profile $c^{FL}(r)$:

$$\frac{d\phi^{FL}}{dr} = -\frac{D_{eff,counterion}^{FL}}{z_{counterion}u_{eff,counterion}^{FL}F}\frac{d\ln c_{H^+}^{FL}}{dr}. \tag{24}$$

Using this equation, it is possible to calculate the molar flux of the protons solely from their concentration gradient:

$$N_{H^+}^{FL} = -\tilde{D}_{eff,H^+}^{FL}\frac{dc_{H^+}^{FL}}{dr} \tag{25}$$

with the effective diffusion coefficient

$$\tilde{D}_{eff,H^+}^{FL} \equiv \frac{z_{counterion}u_{eff,counterion}^{FL}D_{eff,H^+}^{FL} - zH^+u_{eff,H^+}^{FL}D_{eff,counterion}^{FL}}{z_{counterion}u_{eff,counterion}^{FL}} \tag{26}$$

which characterises the whole electrolyte.

Finally, inserting Ohm's law, Equation (17), into the charge balance of the solid matrix, Equation (20), one obtains in dimensionless notation

$$\frac{d^2\Delta\phi^{S^*}}{dr^{*^2}} = -\beta d^{*^2}Ha^2 i_n^*. \tag{27}$$

The parameter β describes the influence of the electric resistance of the solid matrix in relation to the pore diffusion resistance of oxygen and is an analogue to the Prater number known from heterogenous catalysis. Therefore, it is justified to call β the Prater number of the electrochemical reaction (see Table 1).

The dimensionless potential profile of the pore liquid can be obtained from Equation (24) as

$$\frac{d\Delta\phi^{L^*}}{dr^*} = -D_{counterion}^{*}\frac{d\ln c_{H^+}^{*}}{dr^*}. \tag{28}$$

The diffusional and migrational properties of the counterion are lumped in the parameter $D_{counterion}^{*,\infty}$. For very dilute electrolytes the ion mobility of the counterion can be calculated as

$$u_{eff,counterion}^{FL} = \frac{D_{eff,counterion}^{FL}}{RT} \Rightarrow D_{counterion}^{*,\infty} = \frac{1}{z_{counterion}}. \tag{29}$$

In the following, this relation will also be used for electrolyte solutions with medium concentrations as a fair approximation.

For the boundary conditions for the charge transport in the solid matrix, only the ohmic resistance in the matrix has to be accounted for, as long as the resistance in the current collectors (see Figure 1) can be neglected. Charge transfer reactions only occur at the pore walls within the GDE, but not on the GDE's outer surface:

$$-\left.\frac{\mathrm{d}\Delta\phi^{\mathrm{S}^*}}{\mathrm{d}r^*}\right|_{r^*=0} = \frac{\mathrm{d}^*}{1-\mathrm{d}^*}\Delta\phi^{\mathrm{S}^*}(r^*=0);$$
$$-\left.\frac{\mathrm{d}\Delta\phi^{\mathrm{S}^*}}{\mathrm{d}r^*}\right|_{r^*=1} = 0 \qquad (30, 31)$$

Finally, for the charge balance of the pore liquid an initial condition is needed. Here it has to be taken into consideration that the potential difference $\Delta\phi^{\mathrm{FL}}$ is given with respect to a reference electrode RE (see Figure 2), which defines the potential within the liquid bulk. Between there and the edge of the boundary layer (distance d^{RE}), due to the electrolyte resistance, a potential difference proportional to the electric current density occurs (*i*-R-drop)

$$(\phi^{\mathrm{L}})^{\mathrm{L}} - (\phi^{\mathrm{L}})^{\mathrm{RE}} = \frac{d^{\mathrm{RE}}}{\kappa^{\mathrm{L}}} i_{\mathrm{eff}}. \qquad (32)$$

The total potential difference between electrode surface and reference electrode is the sum of the *i*-R-drop, Equation (32), and the concentration overpotential in the liquid film. The latter is obtained from integration of Equation (28). Putting all this together, one gets in terms of the dimensionless numbers:

$$\Delta\phi^{\mathrm{L}^*}(r^*=1) = \ln\left(c^*_{\mathrm{H}^+}(r^*=1)\right)^{-D^*_{\mathrm{counterion}}} + \frac{\rho^*}{\nu_{\mathrm{O}_2}} i^*_{\mathrm{eff}} \qquad (33)$$

with the dimensionless electrolyte resistance ρ^*. The sign of the stoichiometric factor ν_{O2} determines whether an anodic or cathodic current is flowing.

2.1.3. *Reaction microkinetics*

For the local current density of the electrochemical reaction, a Butler–Volmer microkinetic rate expression is applied. In dimensionless notation, it is given by:

$$i^*_n = \exp\left\{\alpha_{\mathrm{a}}\left(\eta^* - \Delta\phi^{\mathrm{S}*} - \Delta\phi^{\mathrm{L}*}\right)\right\}\prod_{j=1}^{N} c_j^{*\,n_{\mathrm{a},j}} - \exp\left\{-\alpha_{\mathrm{c}}\left(\eta^* - \Delta\phi^{\mathrm{S}*} - \Delta\phi^{\mathrm{L}*}\right)\right\}\prod_{j=1}^{N} c_j^{*\,n_{\mathrm{c},j}} \qquad (34)$$

where α_{a} and α_{c} [−] are the charge transfer coefficients of the anodic and the cathodic reactions, respectively, and η^* [−] is the dimensionless reaction overpotential.

The combination of Equations (34), (9) and (10) yields an expression for the effective current density:

$$i^*_{\mathrm{eff}} = D^*\frac{1-d^*}{d^*}\frac{1}{R^{\mathrm{G}}+R^{\mathrm{GL}}+R^{\mathrm{FL}}} = \frac{1-d^*}{\frac{1}{\mathrm{Bi}^{\mathrm{G}}_{\mathrm{m}}}+(1-d^*)+\frac{d^*}{D^*E}}. \qquad (35)$$

The three terms in the denominator, R^{G}, R^{GL} and R^{FL}, are the mass transport resistances in the gas film, the gas layer and the flooded layer, respectively, as well known from classical absorption theory.

To get analytical solutions of the set of differential equations, the concentration profiles in the liquid phase are approximated by piecewise linear profiles as proposed by van Krevelen and Hoftijzer [13, 14]. This leads to the following expression for the enhancement factor

$$E = \frac{\tilde{Ha}_{\mathrm{O}_2}}{\tanh\tilde{Ha}_{\mathrm{O}_2}} \qquad (36)$$

with

$$\tilde{Ha} = d^* Ha\exp\left(-\frac{\alpha_c}{2}\eta^*\right)c^*_{\mathrm{H}^+}(r^*=0) = d^* Ha\exp\left(-\frac{\alpha_c}{2}\eta^*\right)\left(\frac{E_i-E}{E_i-1}c^*_{\mathrm{H}^+}(r^*=1)\right) \qquad (37)$$

The latter is the modified Hatta number for electrochemical oxygen absorption, formulated with respect to the proton concentration on the gas side of the GDE, $c^*_{\mathrm{H}^+}(r^*=0)$, first line, and with respect to the proton concentration on the liquid side, $c^*_{\mathrm{H}^+}(r^*=1)$, second line (positions: see Figure 2).

In Figure 3, simulated polarisation curves are plotted according to Equation (35) under variation of the enhancement factor for the instantaneous reaction E_i. All parameters used are given in Figure 3. Three distinct operating regimes are evident – slow, fast and instantaneous reaction – for which qualitative concentration profiles are also depicted. For low overpotentials (slow reaction), the oxygen reduction kinetics are slow and limit the overall current density. A mass transport limitation can be neglected and the reaction takes place throughout the flooded layer (oxygen concentration profile is decreasing throughout the flooded layer). For higher overpotentials, the reaction rate increases (fast reaction) and the overall process is now increasingly affected by internal mass transport resistances. Therefore in this regime the polarisation curves show a clear dependence on the E_i-factor. The oxygen concentration profile lies much lower than in the previous regime and the oxygen concentration reaches zero within the flooded layer, i.e. the absorbed oxygen is fully consumed. Obviously, the reaction takes place only in a zone near the gas–liquid interface. This zone is the smaller, the higher the overpotential (and therefore the overall reaction rate) is. A further increase in overpotential leads to an instantaneous reaction of oxygen and protons. The reaction zone is compacted to a reaction plane, the process is limited by mass transport of the reactants oxygen and protons only. The different mass

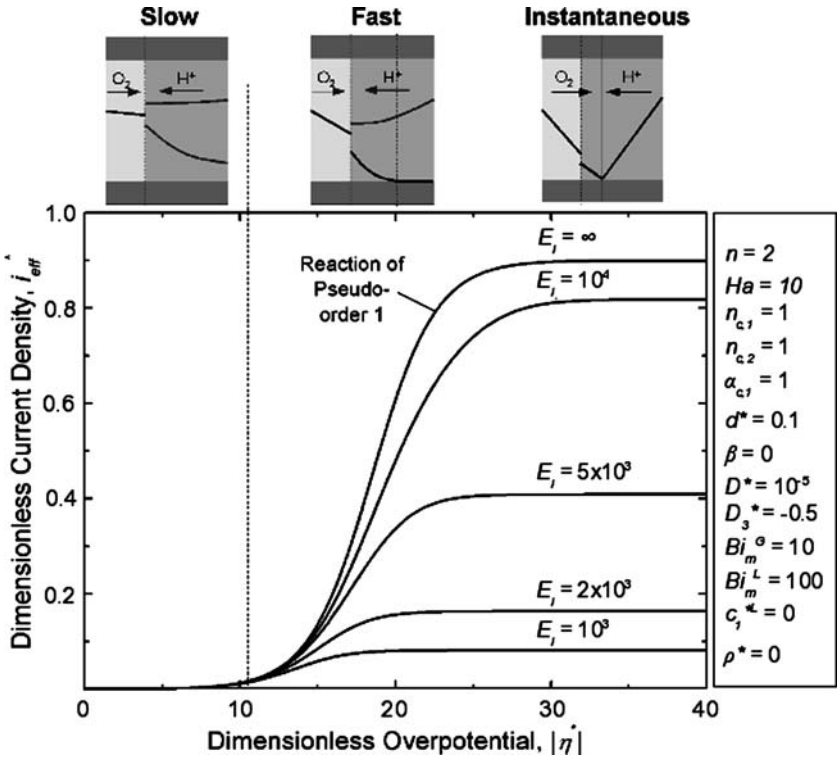

Fig. 3. Simulated polarisation curves according to Equation (35) and qualitative concentration profiles for three different operating regimes.

transport mechanisms determine the location of this reaction plane within the flooded layer. The corresponding current density reaches a limiting value which only depends on the enhancement factor of the instantaneous reaction E_i. The higher this enhancement factor, the higher the effective limiting current density. For an infinite enhancement factor ($E_i \to \infty$), an asymptotic polarisation curve is reached, which corresponds to a pseudo first-order reaction with respect to oxygen.

2.2. *Experimental results*

To validate the model and to identify its parameters, potentiostatic polarisation experiments were performed using the GDEs described in Section 2. The experiments were carried out in a specially designed cyclone flow cell. This provides for a well-defined flow field on both sides of the GDE (comparable to a rotating disk arrangement) and allows the independent adjustment of the outer gas and liquid flow conditions. A detailed description of this cell is given in refs. [15] and [10].

In the experiments, pure oxygen was used. The oxygen flow rate, the total gas pressure and the electrolyte concentration were varied as most important process parameters. The results show that, of these, the electrolyte concentration is most significant. Figure 4 presents some experimental polarisation curves for different electrolyte concentrations. From the model, one would qualitatively expect curves like the dashed one, if a single electrochemical reaction is involved. However, the

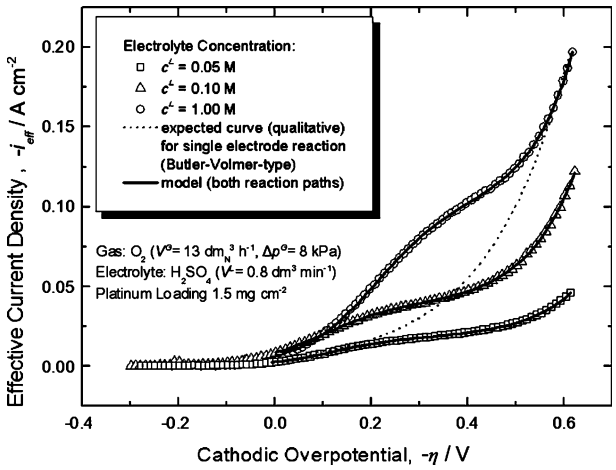

Fig. 4. Experimental polarisation curves for different electrolyte concentrations and qualitative comparison with model Equation (35) (dotted curve).

experimental curves, show a significantly different behaviour. Going from right to left (i.e. from low to high overpotentials), first the current densities increase, but seem to reach an intermediate limiting value, before finally increasing further. This indicates a reaction mechanism which is more complicated than anticipated in the model at this stage.

2.3. *Analysis of oxygen absorption*

According to the literature (e.g. [16]), oxygen reduction in an acidic environment can follow two possible reaction paths: A direct one (upper index "*dir*")

$$O_2(g) + 4e^- + 4H^+ \rightarrow 2H_2O \quad U^\theta = 1.229\,V \tag{38}$$

and an indirect one (upper index "*ind*")

$$O_2(g) + 2e^- + 2H^+ \rightarrow H_2O_2 \quad U^\theta = 0.623\ V$$
$$H_2O_2 + 2e^- + 2H^+ \rightarrow 2H_2O \quad U^\theta = 1.834\ V \tag{39,40}$$

being a consecutive reaction with hydrogen peroxide as intermediate. The direct path is catalysed by platinum, palladium, silver and iron-N_4-chelates and has a standard cell voltage of $U^{\mathrm{dir}}_{i=0} = 1.229$ V. The first step of the indirect path can be observed on carbon surfaces like graphite and carbon black without any metal catalyst, and it has a fairly low standard potential of only $U^{\mathrm{ind}}_{i=0} = 0.623$ V. The hydrogen peroxide decomposition in the second step is catalysed by nickel and cobalt and has a very high standard potential of 1.834 V.

Based on these phenomena, the following assumptions have been made for the modification of the mathematical model:

(a) On the platinum catalyst, oxygen reacts to water using the direct path (4-electron-transfer).
(b) On the carbon black surface, oxygen reacts to hydrogen peroxide (2-electron-transfer).
(c) Hydrogen peroxide decomposition is slow compared to its formation and can be neglected [17].
(d) Far away from the equilibrium potential of the indirect oxygen reduction ($U^\theta = 0.623$ V), the anodic backward reaction can be neglected.
(e) Both reactions microkinetics are described by a Tafel approach with the reaction orders being identical to the stoichiometric coefficients:

$$\text{Direct path:}\quad i^{\mathrm{dir}^*}_{\mathrm{eff}} = -c^*_{O_2}(c_{H^{+*}})^4 \times \exp\left\{-\alpha^{\mathrm{dir}}_c\left[\eta^* - \frac{F}{RT}(U^{\mathrm{dir}}_{i=0} - U^{\mathrm{ind}}_{i=0})\right]\right\} \tag{41}$$

$$\text{Indirect path:}\quad i^{\mathrm{ind}^*}_{\mathrm{eff}} = -c^*_{O_2}(c^*_{H^+})^2 \exp\{-\alpha^{\mathrm{ind}}_c \eta^*\} \tag{42}$$

The overpotential η^* is formulated with respect to the indirect reaction path (see Table 1), therefore in Equation (41) the term $\frac{F}{RT}(U^{\mathrm{dir}}_{i=0} - U^{\mathrm{ind}}_{i=0})$ appears to account for the overpotential of the direct path.

(f) The direct oxygen reduction is slower than the indirect reduction, despite the presence of the platinum catalyst (some orders of magnitude higher carbon surface than platinum surface).

Based on these assumptions, the dimensionless effective current densities of both reaction paths are derived.

2.3.1. *Direct oxygen reduction path (upper index "dir")*

According to Equation (35) the cathodic current density of the direct reduction path can be formulated as

$$i^{\mathrm{dir}^*}_{\mathrm{eff}} = \frac{1-d^*}{\frac{1}{\mathrm{Bi}^{\mathrm{G}}_{\mathrm{m}}} + (1-d^*) + \frac{d^*}{D^* E^{\mathrm{dir}}}} \approx D^* \frac{1-d^*}{d^*} E^{\mathrm{dir}}. \tag{43}$$

As in our experiments pure oxygen is used, no transport limitations occur in the gas phase outside the electrode and consequently the Biot number $\mathrm{Bi}^{\mathrm{G}}_{\mathrm{m}}$ is infinite. Therefore the term in Equation (43) connected with this Biot number vanishes. According to assumption (f) (see list in previuos section) that the direct path only has a moderate reaction rate, the enhancement factor according to Equations (36) and (37) can be approximated by

$$E^{\mathrm{dir}} \approx \tilde{Ha}^{\mathrm{dir}} = d^* Ha^{\mathrm{dir}} \times \exp\left\{-\frac{\alpha^{\mathrm{dir}}_c}{2}\left[\eta^* - \frac{F}{RT}\left(U^{\mathrm{dir}}_{i=0} - U^{\mathrm{ind}}_{i=0}\right)\right]\right\}. \tag{44}$$

As already mentioned in the previous section, Equations (41) and (42), the overpotential η^* is formulated with respect to the indirect reaction path, therefore in Equation (44) the term $\frac{F}{RT}(U^{\mathrm{dir}}_{i=0} - U^{\mathrm{ind}}_{i=0})$ is necessary to obtain the overpotential of the direct path.

2.3.2. *Indirect oxygen reduction path (upper index "ind")*

Following the same argument used for the direct reaction path, the cathodic current density of the indirect reduction path is

$$i^{\mathrm{ind}^*}_{\mathrm{eff}} = \frac{1-d^*}{(1-d^*) + \frac{d^*}{D^* E^{\mathrm{ind}}}} = \frac{1-d^*}{(1-d^*) + \frac{d^*}{D^*}\frac{1-i^{\mathrm{ind}^*}_{\mathrm{eff}}}{E^{\mathrm{ind}}_i - 1} + \frac{1}{D^* Ha^{\mathrm{ind}} \exp\left(-\frac{z^{\mathrm{ind}}_c}{2}\eta^*\right)}} \tag{45}$$

with E^{ind}_i being the enhancement factor of the instantaneous reaction with respect to the concentrations in the liquid bulk and the gas bulk (see explanation in Table 1). In the denominator of Equation (45) three resistance terms are summed up (from left to right):

- the diffusion resistance of oxygen in the gas-filled pores of the electrode,
- the diffusion resistance of the protons in the liquid-filled pores of the electrode and
- the combination of the resistances of the electrochemical reaction and the diffusion of oxygen in the liquid phase.

For high overpotentials η^* the latter resistance vanishes and the current density reaches one of two

possible limiting values, depending on the enhancement factor:

$$i_{\mathrm{eff,lim}}^{\mathrm{ind}*} \equiv \frac{i_{\mathrm{eff,lim}}^{\mathrm{ind}}}{i_{\mathrm{eff,max}}^{\mathrm{ind}}} = \left\{ \begin{array}{cc} D^* \frac{1-d^*}{d^*} E_i^{\mathrm{ind}} & \text{for } E_i^{\mathrm{ind}} < \frac{d^*}{D^*(1-d^*)} \\ 1 & \text{for } E_i^{\mathrm{ind}} \geq \frac{d^*}{D^*(1-d^*)} \end{array} \right\} \tag{46}$$

This dependence is shown in Figure 5. For comparison three effective limiting current densities are plotted. These were calculated from a fit of the model for the indirect path, Equation (45), to the experimental polarisation curves given in Figure 4, for low overpotentials. The model shows good agreement with the experiments.

2.3.3. *Formulation of the overall current density*

The overall current density is given as the sum of the current densities of both reaction paths:

$$\begin{aligned} i_{\mathrm{eff}} &= i_{\mathrm{eff}}^{\mathrm{dir}} + i_{\mathrm{eff}}^{\mathrm{ind}} \\ &= B_1 \exp\left\{ -\frac{\alpha_c^{\mathrm{dir}}}{2} \left[\eta^* - \frac{F}{RT} \left(U_{i=0}^{\mathrm{dir}} - U_{i=0}^{\mathrm{ind}} \right) \right] \right\} \\ &\quad + \frac{1}{\frac{1}{i_{\mathrm{eff,lim}}^{\mathrm{ind}}} + \frac{1}{B_2 \exp\left(-\frac{\alpha_c^{\mathrm{ind}}}{2} \eta^* \right)}} \end{aligned} \tag{47}$$

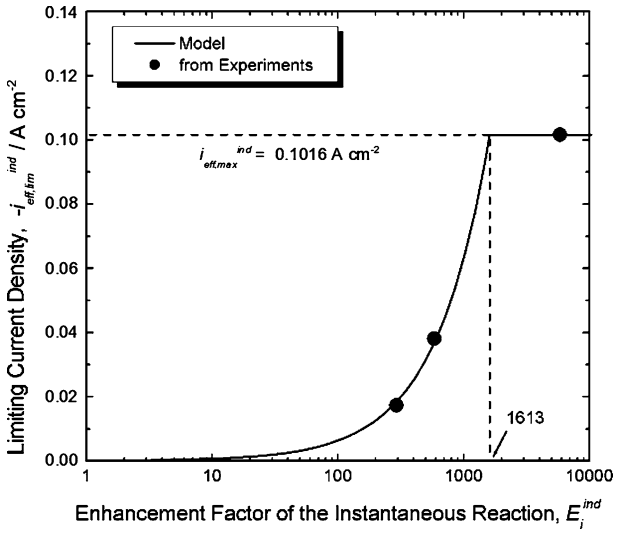

Fig. 5. Effective limiting current density as function of the enhancement factor of the instantaneous reaction, comparison between model, Equation (46), and values calculated from experimental data.

$$\text{with} \quad B_1 = 2 i_{\mathrm{eff,max}}^{\mathrm{ind}} D^* (1 - d^*) Ha^{\mathrm{dir}} \tag{48}$$

$$\text{and} \quad B_2 = i_{\mathrm{eff,max}}^{\mathrm{ind}} D^* (1 - d^*) Ha^{\mathrm{ind}} \tag{49}$$

In the experiments, the overall current density is measured as a function of the electrode potential. According to Equation (47) the following five parameter groups determine this dependence:

- the group B_1 representing the reaction rate of the direct oxygen reduction,
- the group B_2 representing the reaction rate of the indirect oxygen reduction,
- the limiting current density of the indirect oxygen reduction $i_{\mathrm{eff,lim}}^{\mathrm{ind}}$,
- the cathodic charge transfer coefficient of the direct oxygen reduction $\alpha_{\mathrm{c}}^{\mathrm{dir}}$,
- the cathodic charge transfer coefficient of the indirect oxygen reduction $\alpha_{\mathrm{c}}^{\mathrm{ind}}$.

Their values are given in Table 2, determined by non-linear regression of experimental polarisation data for three different proton concentrations in the liquid phase. The simulation results show excellent agreement with the experimental observations, as can be seen in Figure 4 (solid curves).

The superposition of both reaction paths contributions to the overall current density is shown in Figure 6. For low overpotentials, only the indirect path contributes to the cell current and finally reaches its limiting current density. For higher overpotentials direct oxygen reduction also occurs and dominates the process for high overpotentials. Within the plotted region, it does not reach its limiting current density. The reason why the limiting current density of the indirect path lies much lower than that of the direct path is most likely the slow decomposition of hydrogen peroxide combined with the strong adsorption of hydrogen peroxide on carbon surfaces. Therefore it can be assumed, that under steady conditions most of the carbon surface is covered with hydrogen peroxide.

2.3.4. *Oxygen transport in the gas-filled pores*

With the help of the identified parameters (Table 2) and Equations (1) and (45), the maximum limiting current density of the indirect oxygen reduction can be

Table 2. Enhancement factors E_i^{ind} and model parameters for three selected proton concentrations derived from non-linear regression (Confidence intervals valid for a confidence number of 95%), and ratio of exchange current densities calculated from Equation (55)

Parameter	$c_{\mathrm{H+}}^{\mathrm{L}} = 0.1$ mol dm^{-3}	$c_{\mathrm{H+}}^{\mathrm{L}} = 0.2$ mol dm^{-3}	$c_{\mathrm{H+}}^{\mathrm{L}} = 2.0$ mol dm^{-3}
E_i^{ind}	293	585	5836
$-B_1$ / A cm^{-2}	$0.93\times10^{-6} \pm 0.11\times10^{-6}$	$1.12\times10^{-6} \pm 0.09\times10^{-6}$	$6.48\times10^{-8} \pm 1.67\times10^{-8}$
$-B_2$ / A cm^{-2}	$1.64\times10^{-2} \pm 0.04\times10^{-2}$	$3.07\times10^{-2} \pm 0.05\times10^{-2}$	$4.11\times10^{-3} \pm 0.18\times10^{-3}$
$-i_{\mathrm{eff,lim}}^{\mathrm{ind}}$ / A cm^{-2}	0.0173 ± 0.0003	0.0381 ± 0.0005	0.1016 ± 0.0015
$\alpha_{\mathrm{c}}^{\mathrm{dir}}$	0.48 ± 0.01	0.50 ± 0.01	0.58 ± 0.02
$\alpha_{\mathrm{c}}^{\mathrm{ind}}$	0.76 ± 0.02	0.69 ± 0.02	0.67 ± 0.01
$(ai_0)^{\mathrm{dir}}/(ai_0)^{\mathrm{ind}}$	1.7×10^{-9}	0.6×10^{-10}	1.2×10^{-10}
$(ai_0)^{\mathrm{ind}}$ / A m^{-3}	5.7×10^{10}	19.9×10^{10}	3.6×10^{9}

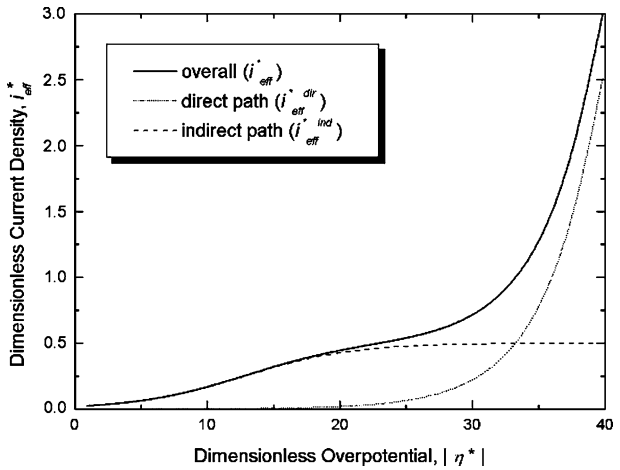

Fig. 6. Simulated polarisation curve using the final model, Equation (47): Superposition of both reaction paths of the oxygen reduction.

calculated: $\left|i^{\text{ind}}_{\text{eff,max}}\right| = 0.1016$ A cm^{-2}. From this it is possible to estimate the diffusion coefficient of oxygen in the gas filled pores of the electrode (gas layer), assuming that the penetration of the liquid phase is small ($d^{\text{FL}} \ll d$) due to the hydrophobicity of the electrode matrix:

$$D^{\text{GL}}_{\text{O}_2} = \frac{D^{\text{GL}}_{\text{eff,O}_2}}{\varepsilon^{1.5}} = \frac{-i^{\text{ind}}_{\text{eff,max}} d}{2\varepsilon^{1.5} p^{\text{G}}_{\text{O}_2} F/(RT)} \approx 2.77 \times 10^{-7}\,\text{m}^2\,\text{s}^{-1} \tag{50}$$

This value indicates that within the electrode oxygen is mainly transported via Knudsen diffusion. The pore equivalent diameter for oxygen can therefore be calculated from the molar mass of oxygen, M_{O2} [kg mol^{-1}], using Knudsen's equation

$$d_{\text{p,eq}} = \frac{3}{2} D^{\text{GL}}_{\text{O}_2} \sqrt{\frac{\pi}{2} M_{\text{O}_2}} = 1.9\,\text{nm} \tag{51}$$

Obviously, oxygen is transported through the micropores of the electrode.

Finally, by rearranging Equation (46) one obtains an expression for the dimensionless thickness of the flooded layer as a function of the enhancement factor of the instantaneous reaction E^{ind}_i and the effective limiting current density of the indirect path $i^{\text{ind}}_{\text{eff,lim}}$:

$$d^* = \frac{D^*}{D^* + \frac{1}{E^{\text{ind}}_i} \frac{i^{\text{ind}}_{\text{eff,lim}}}{i^{\text{ind}}_{\text{eff,max}}}} \tag{52}$$

According to Equation (46), the maximum current density $i^{\text{ind}}_{\text{eff,lim}} = i^{\text{ind}}_{\text{eff,max}}$ is reached for enhancement factors of the instantaneous reaction of $E^{\text{ind}}_i = 1613$ and higher. Inserting this into Equation (52), the thickness of the flooded layer can be calculated:

$$d^* \equiv \frac{d^{\text{FL}}}{d} = \frac{D^*}{D^* + 1/1613} = 0.225 \tag{53}$$

$$\text{with} \quad D^* \equiv \frac{D^{\text{FL}}_{\text{eff,O}_2} c^{\text{Le}}_{\text{O}_2}(p^{\text{G}}_{\text{O}_2})}{D^{\text{GL}}_{\text{eff,O}_2} p^{\text{G}}_{\text{O}_2}/(RT)} = 1.8 \times 10^{-4} \tag{54}$$

Therefore, under the given experimental conditions, the liquid phase only penetrates less than a quarter of the electrode thickness, approximately fulfilling the assumption of low penetration.

2.3.5. *Analysis of exchange current densities*

From the values of the parameter groups B_1 and B_2 (Table 2) the ratio of the exchange current densities of the direct and the indirect oxygen reduction can be calculated as

$$\frac{(ai_0)^{\text{dir}}}{(ai_0)^{\text{ind}}} = \frac{(Ha^{\text{dir}})^2 4F}{(Ha^{\text{ind}})^2 2F} = \frac{1}{2}\left(\frac{B_1}{B_2}\right)^2 \tag{55}$$

The values are also given in Table 2, as well as the exchange current densities of the indirect oxygen reduction, calculated from the parameter group B_2:

$$(ai_0)^{\text{ind}} = \frac{2FD^{\text{L}}_{\text{eff,O}_2} c^{\text{Le}}_{\text{O}_2}(p^{\text{G}}_{\text{O}_2})(B_2)^2}{(i^{\text{ind}}_{\text{eff,max}}(1-d^*)D^* d)^2} \tag{56}$$

It can be seen from these results, that the exchange current densities of the direct oxygen reduction to water are much smaller than those of the indirect reduction to hydrogen peroxide. This has two reasons: on one hand, the activity of platinum as catalyst for the direct oxygen reduction is low. On the other hand, the platinum surface is small compared to that of the carbon black surface.

2.3.6. *Analysis of charge transfer coefficients*

Also given in Table 2 are the charge transfer coefficients of the direct and the indirect reaction path of the electrochemical oxygen reduction, $\alpha^{\text{dir}}_{\text{c}}$ and $\alpha^{\text{ind}}_{\text{c}}$, for three different proton concentrations. The values for the direct path, $\alpha^{\text{dir}}_{\text{c}}$, are very close to the ideal theoretical value of 0.5 which leads to the conclusion that the derived Butler–Volmer-type reaction rate expression, Equation (43), describes the process very accurately. The charge transfer coefficients of the indirect path, $\alpha^{\text{ind}}_{\text{c}}$, have slightly higher values of around 0.7. This leads to the conclusion, that the derived rate expression, equation (45), is also a reasonable description of the underlying process, but the approximation is not as good as for the direct path. Obviously some of the assumptions made for formulating the model with respect to the indirect path have to be more closely checked. Further experimental results not mentioned in this paper show, that there is a slight influence of the flow velocity in the liquid bulk. The higher the liquid flow velocity, the lower are the current densities. This is plausible, considering the influence of peroxide decomposition, which has been neglected during the derivation of the model. The higher the liquid flow velocity, the more peroxide is transported away from the electrode surface. Consequently, less peroxide is available for the decomposition reaction and therefore the contribution of this reaction to the overall current is reduced.

3. Conclusions

It can be concluded that oxygen transport in the gas-filled part of the GDE pore structure is controlled by Knudsen diffusion in the micropores. Due to the hydrophobicity of the electrode material, the liquid phase only penetrates the macropores with a total penetration depth of less than 25% of the electrode thickness.

Furthermore, it was confirmed that the electrochemical oxygen reduction follows a parallel reaction scheme forming hydrogen peroxide at the carbon black support (indirect path), and water at the platinum catalyst particles (direct path), with the indirect path being the dominating reaction for low overpotentials.

Even though hydrogen peroxide decomposition was neglected for this first model approach, good agreement with the experimental data was achieved.

With the help of the proposed model for the transport and reaction processes, proton concentrations can be estimated, for which a maximum current density is achieved. This is the key for the estimation of the most important electrode parameter: the diffusion coefficient of the gaseous reactant in the gas-filled part of the electrode.

Finally, it can be concluded that the derived analytical model equations are applicable for the design of electrochemical reactors for gas absorption based on GDEs. Also the classical film theory of chemical absorption is extendable to electrochemical absorption processes.

References

1. Staab, D. Bergner and K. Hannesen, European Patent EP-PS 182 114, 26.10.1984, Hoechst AG.
2. D. Bergner, *Chem.-Ing.Tech.* **69** (1997) 438.
3. Wiesener, Experimentelle Untersuchungen zur Anwendung von Sauerstoffdiffusionselektroden bei der Synthese von Metallsalzlösungen für die Galvanotechnik unter Vermeidung von Abfallprodukten, Abschlußbericht zum AiF-Forschungsvorhaben Nr. 9127 B (Meinsberg, 1995) pp. 1–97.
4. J.C. Card, S.E. Lyke and S.H. Langer, *J. Appl. Electrochem.* **20** (1990) 269.
5. T.D. Tran, I. Londoner and S.H. Langer, *Electrochim. Acta* **38** (1993) 221.
6. G.R. Dieckmann and S.H. Langer, *J. Appl. Electrochem.* **27** (1997) 1.
7. M.S. Saha, A. Denggerile, Y. Nishiki, T. Furuta and T. Ohsaka, *Electrochem. Comm.* **5** (2003) 445.
8. L. Carrette, K.A. Friedrich and U. Stimming, *Fuel Cells* **1**(1) (2001) 5.
9. O. Nowitzki, R. Hamelmann, K. Sundmacher and U. Hoffmann, 'Production of Gas-Diffusion-Electrodes loaded with Non-noble Metal Catalyst for Oxygen Reduction by a Calandering Rolling Process,' in I. Rousar (ed), *Contemporary Trends in Electrochemical Engineering* , (UTAX, Prague, 1996) pp. 227–233.
10. K. Sundmacher and T. Schultz, *Chem. Eng. J.* **82** (2001) 117.
11. K. Sundmacher and U. Hoffmann, *J. Appl. Electrochem.* **28** (1998) 359.
12. J.S. Newman, *Electrochemical Systems*, 2nd ed., (Prentice Hall, Englewood Cliffs, New Jersey, 1991), pp. 461.
13. D.W. Van Krevelen and P.J. Hoftijzer, *Rec. Trav. Chim. Pays-Bas.* **67** (1948) 563.
14. K.R. Westerterp, P.M. van Swaaij and A.A.C.M. *Beenackers, Chemical Reactor Design and Operation*, Student ed. (Wiley, Chichester, 1990) pp. 400–403.
15. K. Sundmacher, *J. Appl. Electrochem.* **29** (1999) 919.
16. K. Kinoshita, *Electrochemical Oxidation Technology* (Wiley, New York, 1992), pp. 19–20.
17. J.S. Newman, *Electrochemical Systems*, 2nd ed., (Prentice Hall, Englewood Cliffs, New Jersey, 1991), pp. 201–202.